

The Effect of Tropospheric Jet Latitude on Coupling between the Stratospheric Polar Vortex and the Troposphere

CHAIM I. GARFINKEL AND DARRYN W. WAUGH

Department of Earth and Planetary Science, The Johns Hopkins University, Baltimore, Maryland

EDWIN P. GERBER

Center for Atmosphere Ocean Science, Courant Institute of Mathematical Sciences, New York University, New York, New York

(Manuscript received 23 May 2012, in final form 6 September 2012)

ABSTRACT

A dry general circulation model is used to investigate how coupling between the stratospheric polar vortex and the extratropical tropospheric circulation depends on the latitude of the tropospheric jet. The tropospheric response to an identical stratospheric vortex configuration is shown to be strongest for a jet centered near 40° and weaker for jets near either 30° or 50° by more than a factor of 3. Stratosphere-focused mechanisms based on stratospheric potential vorticity inversion, eddy phase speed, and planetary wave reflection, as well as arguments based on tropospheric eddy heat flux and zonal length scale, appear to be incapable of explaining the differences in the magnitude of the jet shift. In contrast, arguments based purely on tropospheric variability involving the strength of eddy–zonal mean flow feedbacks and jet persistence, and related changes in the synoptic eddy momentum flux, appear to explain this effect. The dependence of coupling between the stratospheric polar vortex and the troposphere on tropospheric jet latitude found here is consistent with 1) the observed variability in the North Atlantic and the North Pacific and 2) the trend in the Southern Hemisphere as projected by comprehensive models.

1. Introduction

It is now well established that the stratospheric polar vortex can influence tropospheric weather and climate. Baldwin and Dunkerton (1999) and Limpasuvan et al. (2004) illustrate the impact of natural variations of the polar vortex on tropospheric variability. Extended range forecasts are improved with better initialization and representation of the stratosphere (e.g., Baldwin et al. 2003; Roff et al. 2011). Climatological changes in the Southern Hemisphere (SH) stratospheric vortex associated with ozone loss have had a profound impact on SH climate, from Antarctica (e.g., Thompson et al. 2011) to the subtropics (e.g., Kang et al. 2011). Climate change simulations require accurate treatment of stratospheric ozone to capture recent trends (e.g., Arblaster and Meehl 2006; Son et al. 2010; Polvani et al. 2011).

This study will focus on how differences in the climatological latitude of the tropospheric midlatitude jet may influence its response to anomalies in the lower stratospheric polar vortex. A colder, stronger stratospheric vortex is associated with a poleward shift of the tropospheric jet stream (e.g., Polvani and Kushner 2002, hereafter PK02) but the magnitude of the tropospheric jet shift for a given change in the stratospheric vortex varies considerably in different regions of the globe and across different model simulations. In both observations and models, however, there is a remarkable connection between the latitude of the jet stream and the magnitude of its response to the vortex. As motivation for this study, we present two examples.

First, the SH midlatitude jet in current climate models is generally biased toward low latitudes relative to observations (in which the jet latitude is poleward of 50°; e.g., Fyfe and Saenko 2006). The magnitude of the midlatitude SH jet shift in response to ozone loss or increased CO₂ in each model appears to sensitively depend on the magnitude of this bias. Kidston and Gerber (2010), Barnes and Hartmann (2010), and Son et al. (2010) find that in models in which the SH

Corresponding author address: Chaim I. Garfinkel, Department of Earth and Planetary Science, The Johns Hopkins University, Baltimore, MD 21209.
E-mail: cig4@jhu.edu

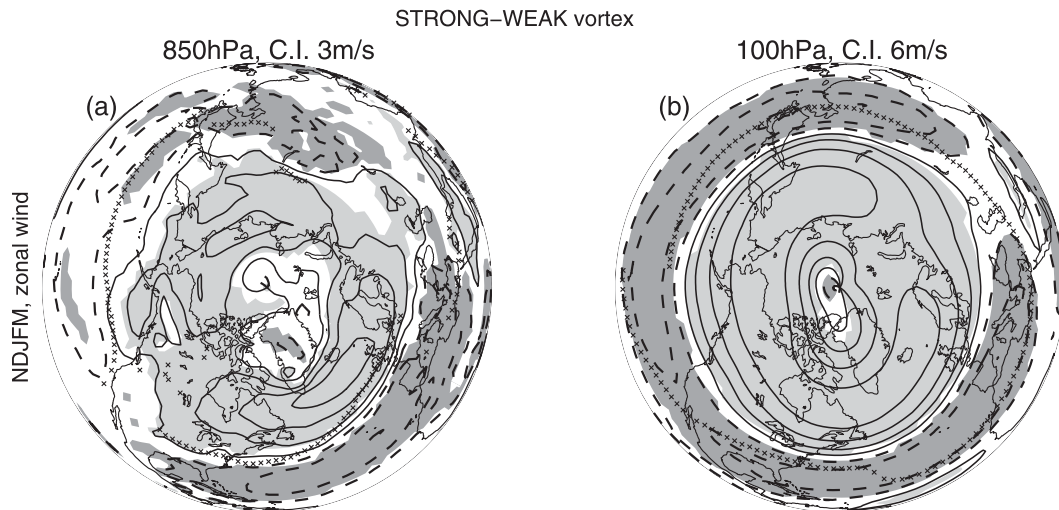


FIG. 1. Difference in zonal wind between November and March months with an anomalously strong and an anomalously weak vortex. Asterisks mark the climatological jet maximum at each longitude. Months are composited if geopotential height anomalies area and height averaged from 65°N to the pole and from 70 to 150 hPa exceed 0.5 standard deviations.

midlatitude jet is too far equatorward, the response to an external forcing (either increased CO₂ or ozone loss) is magnified. Thus, many models may be predicting too large a shift in the SH circulation in response to increased CO₂ or ozone loss.

Second, while anomalies in the Northern Hemisphere (NH) polar vortex are largely zonally symmetric, the response in the midlatitude Atlantic sector (where the jet latitude is 40°–45°) is stronger than the response in the midlatitude Pacific sector (where the jet latitude is 30°–35°). Figure 1 shows the difference in NH zonal wind between months with an anomalously strong vortex and months with an anomalously weak vortex, where strong anomalies are characterized by months that exceed ± 0.5 standard deviations. In the lower troposphere (Fig. 1a), the effect of the vortex is clearly stronger in the North Atlantic where the jet is farther poleward. If we average the change in jet latitude in each sector, the change in jet latitude at 850 hPa between 150° and 230°E (in the Pacific sector) is 0.9°, while the change in jet latitude between 300° and 20°E (in the Atlantic sector) is 5.5°. The jet latitude is calculated as in section 2. This difference between the sectors is robust to altered definitions of strong and weak vortex events, to excluding midwinter so that the dominant mode of variability is qualitatively similar between the sectors (Fig. 13 of Eichelberger and Hartmann 2007), and to altered definitions of the sectors (not shown). Furthermore, Breiteig (2008), Newman and Sardeshmukh (2008), Garfinkel and Hartmann (2011b, their Fig. 9), Limpasuvan et al. (2004, their Figs. 6 and 9), Baldwin et al. (2003, their Fig. 3), and Baldwin and Dunkerton (2001) all also indicate that the

effect of vortex variability in the troposphere is stronger in the Atlantic.

Changes in the jet position impact other aspects of the climate system (e.g., subtropical precipitation; Polvani et al. 2011). Thus, differences in the jet position between sectors or between models may significantly affect predictions on both seasonal and decadal time scales. It is therefore important to understand how and why the response to a polar vortex depends on jet structure.

Simplified dry general circulation models (sGCMs) have been used extensively to study jet variability, including the feedback between eddies and the mean state that sets the time scales of the annular modes in the troposphere (Yu and Hartmann 1993; Gerber and Vallis 2007; Eichelberger and Hartmann 2007; Son et al. 2008) and the influence of the stratosphere on tropospheric jets (PK02; Kushner and Polvani 2004; Garfinkel and Hartmann 2011a). A few recent studies have connected these themes. Chan and Plumb (2009) show that the magnitude of the tropospheric response to a polar vortex is highly sensitive to the persistence of the annular mode. If the intrinsic variability is bimodal, as it was in the experiments of PK02, the tropospheric response to a vortex is unrealistically large. Simpson et al. (2010, 2012) have examined the response to tropical heating in the lower stratosphere (intended to mimic the effect of the solar cycle) in an sGCM with 15 vertical levels. They find that both the annular mode persistence and the response to a stratospheric forcing increase for more equatorward jets. The sensitivity is closely related to changes in eddy–mean flow feedbacks. The importance of tropospheric eddy feedback on the response to stratospheric

perturbations was also suggested by Hartmann et al. (2000) and investigated in idealized models by Song and Robinson (2004) and Kushner and Polvani (2004).

We use an sGCM to understand how jet latitude impacts stratosphere–troposphere coupling. Even though the jets in the North Pacific, North Atlantic, and SH differ by more than jet latitude (e.g., strength, amount of eddy activity, southwest–northeast tilt of the Atlantic jet), our SGCM experiments isolate and demonstrate the importance of differences in jet latitude. We show that a jet located near 40° responds most strongly to changes in the stratospheric vortex, while jets near 50° and 30° respond nearly identically to vortex perturbations. A number of mechanisms have been proposed to explain how a stratospheric perturbation influences the troposphere, but no one, to the authors' knowledge, has tried to systematically compare them against each other in a quantitative sense in order to deduce which one(s) are most important. We will show that *stratospheric* focused arguments involving eddy phase speed, stratospheric potential vorticity (PV) inversion, and planetary wave reflection, as well as arguments involving tropospheric eddy heat fluxes and eddy length scales, fail to explain the differences in the magnitude of the jet shift. In contrast, arguments involving the strength of *tropospheric* eddy feedback, and in particular of high-frequency synoptic eddy momentum fluxes, appear to explain the magnitude of the jet shift. While this does not necessarily disprove any of the other mechanisms, this does confirm that *tropospheric* eddy feedbacks are essential to understanding the response of the mid-latitude jets to stratospheric perturbations. Tropospheric eddy feedbacks bury the initial signal connecting the stratospheric perturbation to the troposphere, making it very difficult to determine how the stratosphere affected the troposphere in the first place.

Gerber et al. (2008), Barnes and Hartmann (2010), Kidston and Gerber (2010), and Son et al. (2010) confirmed a link among jet latitude, jet persistence (as quantified by the annular mode time scale), and the jet shift in response to an external perturbation in models. In these studies, however, it was not possible to establish causality between jet persistence and the magnitude of a jet shift, as the jet latitude and jet persistence were monotonically related. That is to say, it is unclear whether it is changes in the eddy feedback that actually control the magnitude of the jet shift. As discussed in Kidston and Gerber (2010), a simple geometric argument might explain why jets with a low-latitude bias are more sensitive to external perturbation: spherical geometry limits the poleward extension of the jet, leaving more room for a jet initially at 30° to move, as compared to a jet that is initially at 50°. Here we establish a system with a

nonmonotonic link between annular mode time scales and jet latitude, and demonstrate that the former matters most.

After discussing the dry model parameterizations and our diagnostics (section 2), we introduce model configurations where the position of the eddy-driven jet stream is varied from 30° to 50° (section 3). We then demonstrate that the response of the jet to the stratospheric perturbation depends nonmonotonically on the jet latitude (section 4) and discuss possible mechanisms for this dependence (sections 5 and 6). We conclude in section 7.

2. Methodology

a. The idealized dry model

The Geophysical Fluid Dynamics Laboratory (GDFL) spectral atmospheric dynamical core is used to isolate the relationship between the climatological position of the tropospheric jet and its response to stratospheric perturbations. The model parameterizations in the troposphere follow Held and Suarez (1994, hereafter HS94) except for the following modifications. HS94 specify the tropospheric temperature profile as

$$T_{\text{eq}}^{\text{trop}}(p, \phi) = \max \left[200 \text{ K}, (T_0 - \delta T_{\text{HS94}}) \left(\frac{p}{p_0} \right)^{\kappa} \right], \quad (1)$$

where $\delta T_{\text{HS94}} = (\Delta T)_y \sin^2 \phi + (\Delta T)_z \log(p/p_0) \cos^2 \phi$, $T_0 = 315 \text{ K}$, $p_0 = 1000 \text{ hPa}$, $(\Delta T)_y = 60 \text{ K}$, and $(\Delta T)_z = 10 \text{ K}$, where we use the same notation as HS94. Two additional terms are added onto δT_{HS94} to form δT_{new} , which replaces δT_{HS94} in Eq. (1):

$$\begin{aligned} \delta T_{\text{new}} = & \delta T_{\text{HS94}} + A \cos[2(\phi - 45)]P(\phi) \\ & + B \cos[2(\phi - 45)] \sin[3(\phi - 60)] \\ & \times \left\{ \exp \left[-\frac{(\phi - 15)^2}{2 * 15^2} \right] + \exp \left[-\frac{(\phi + 15)^2}{2 * 15^2} \right] \right\}, \end{aligned} \quad (2)$$

where $P(\phi) = \sin[4(\phi - 45)]$ or $P(\phi) = \sin(4\phi - 45)$. Note that increasing A and B shifts the jet poleward. By modifying the values of A , B , and the form of $P(\phi)$, the tropospheric baroclinicity, and thus the climatological position of the jet, can be shifted meridionally. However, the equator-to-pole temperature difference does not change with A , B , or $P(\phi)$. Section 3 will show that this leads to heat fluxes and maximum jet speeds that are nearly equal in strength among all the integrations, two traits we consider desirable.

A more realistic stratosphere is created following PK02. Above 100 hPa, the equilibrium temperature profile is

given by $T_{\text{eq}}^{\text{strat}}(p, \phi) = [1 - W(\phi)]T_{\text{US}}(p) + W(\phi)T_{\text{PV}}(p)$ where T_{US} is the U.S. Standard Temperature,

$$T_{\text{PV}}(p) = T_{\text{US}}(p_T) \left(\frac{p}{p_T} \right)^{R\gamma/g} \quad (3)$$

is the temperature of an atmosphere with a constant lapse rate γ (K km^{-1}), and $W(\phi)$ is a weight function that confines the cooling over the North Pole:

$$W(\phi) = \frac{1}{2} \left\{ 1 - \tanh \left[\frac{(\phi - \phi_0)}{\delta\phi} \right] \right\}, \quad (4)$$

with $\phi_0 = 50$ and $\delta\phi = 10$. By modifying the values of γ and ϕ_0 , the strength and meridional extent of the polar vortex can be controlled. To assess the robustness of our results to polar stratospheric vortex width, a few integrations are conducted with ϕ_0 from Eq. (4) set to 40. Wavenumber-2 topography that is 6 km high from peak to trough is added in the hemisphere where the vortex is imposed following Gerber and Polvani (2009) in order to excite more realistic variability and to help eliminate regime behavior in the troposphere. Except where indicated, all figures and discussion in this paper are for the hemisphere with the topography and vortex.

Each unique tropospheric configuration [unique combination of A , B , and $P(\phi)$] will be referred to as an *experiment*. For each experiment, a pair of integrations is performed: one with $\gamma = 0$ and the other with $\gamma = 6$, in Eq. (3). Table 1 lists the key parameterizations for each integration. The experiment denoted J30 (i.e., jet near 30°) is identical to cases 7 and 10 of Gerber and Polvani (2009) except that we set the asymmetry factor between the two hemispheres [ϵ in Eq. (A4) of PK02] to 0 so that the equator-to-pole temperature difference is constant in both hemispheres. Two additional experiments are denoted J40 and J50 (i.e., jets near 40° and 50°), corresponding to the approximate jet latitude of observed wintertime jets in the North Atlantic and SH. Figure 2 shows the surface equilibrium temperature profile for the J30, J40, and J50 cases.

One final tropospheric configuration is explored. Gerber and Vallis (2007) and Simpson et al. (2010) (their TR1) analyze a case in which the equator-to-pole temperature difference is set to 40 K. To ease comparison between our results and theirs, we also perform an experiment (i.e., pair of integrations $\gamma = 0$ and $\gamma = 6$) with the equator-to-pole temperature difference set to 40 K, but with topography, 40 vertical levels, and a PK02 stratosphere as in all other cases presented in this paper (denoted $\Delta T40$ and listed in Table 1).

The sigma vertical coordinate has 40 vertical levels defined as in PK02. Model output data on sigma levels are interpolated to pressure levels before any analysis is

performed. The ∇^8 hyperdiffusion in the model selectively damps the smallest-scale spherical harmonic at a time scale of 0.1 days. The model output is sampled daily. The horizontal resolution is T42; however, a few experiments are conducted at T63 resolution in order to assess the robustness of our results to model resolution. Note that stratosphere–troposphere coupling on intra-seasonal time scales is inhibited in the $\gamma = 0$ integration, as Rossby waves do not deeply penetrate the stratosphere (e.g., Fig. 6b of Gerber 2012). Coupling does occur in the $\gamma = 6$ integration, but the strong vortex inhibits stratospheric sudden warmings (Gerber and Polvani 2009).

TABLE 1. Different experiments performed for understanding the response in the troposphere to imposing a polar stratospheric vortex. The integration length gives the duration in days after discarding the first 400 days of the integration, and the 2x indicates that a strong vortex and a no vortex (i.e., $\gamma = 0$ and $\gamma = 6$) integration has been performed for the tropospheric parameter setting. Note that jet latitude increases along with A and B . Setting $P(\phi) = \sin(4\phi - 45)$ leads to a slightly stronger subtropical baroclinicity and subtropical jet in the cases equatorward of J30 in Fig. 6a. Note that Simpson et al. (2010) shift the latitude of the tropospheric jet by setting $A = \pm 2$ for their TR2 and TR4 cases. Two classes of sensitivity experiments have been performed—the first at T63 resolution and the second with a vortex width of $\phi_0 = 40$ —for the J30, J40, and J50 cases; these experiments are not included on this table.

Dry model tropospheric parameter settings				
Experiment	A	B	$P(\phi)$ in Eq. (2)	Integration length
J30	0	0	N.A.	5100
	−10	0	$\sin(4\phi - 45)$	2×5100
	−5	0	$\sin(4\phi - 45)$	2×5100
	5	0	$\sin(4\phi - 45)$	2×9400
	10	0	$\sin(4\phi - 45)$	2×5100
	5	0	$\sin[4(\phi - 45)]$	$2 \times 15\ 100$
	10	0	$\sin[4(\phi - 45)]$	2×5100
J40	5	4	$\sin[4(\phi - 45)]$	2×9400
	5	8	$\sin[4(\phi - 45)]$	2×9400
	5	12	$\sin[4(\phi - 45)]$	2×5100
	5	16	$\sin[4(\phi - 45)]$	2×5100
J50	5	20	$\sin[4(\phi - 45)]$	2×5100
$\Delta T40$	0	0	$\Delta T = 40\ \text{K}$, $T_{\text{max}} = 305\ \text{K}$	2×9400

performed. The ∇^8 hyperdiffusion in the model selectively damps the smallest-scale spherical harmonic at a time scale of 0.1 days. The model output is sampled daily. The horizontal resolution is T42; however, a few experiments are conducted at T63 resolution in order to assess the robustness of our results to model resolution. Note that stratosphere–troposphere coupling on intra-seasonal time scales is inhibited in the $\gamma = 0$ integration, as Rossby waves do not deeply penetrate the stratosphere (e.g., Fig. 6b of Gerber 2012). Coupling does occur in the $\gamma = 6$ integration, but the strong vortex inhibits stratospheric sudden warmings (Gerber and Polvani 2009).

The minimum integration length for each experiment is 5100 days. Simpson et al. (2010) argue that very long integrations are necessary to precisely measure either the magnitude of a jet shift in response to an external forcing or the annular mode persistence time scale. We expect that if our integrations were extended for longer, some of the intra-ensemble scatter might be reduced. In addition, we do extend the integrations with large jet persistence up to 15 100 days (see Table 1). However, our approach is to create a continuum of experiments in which the baroclinic forcing gradually moves the jet from near 25° to near 55° . Were we to combine similar experiments together, we would have at least 30 000

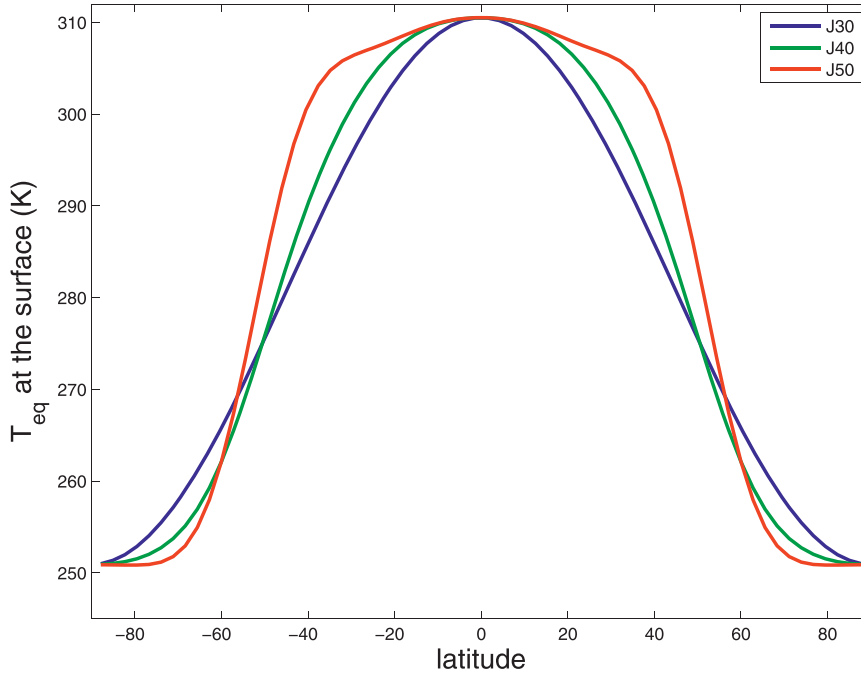


FIG. 2. Surface temperature toward which the model is relaxed for the J30, J40, and J50 cases.

days of sGCM output for experiments with jets centered near 30°, 40°, and 50°.

In summary, we seek to vary the position of the eddy-driven jet in the troposphere and the strength of the polar vortex in the stratosphere. The key parameters of the study are A and B , which vary the tropospheric temperature gradient; γ , which varies the strength of the stratospheric vortex; and ϕ_0 , which controls the width of the vortex.

b. Diagnostics

Several diagnostics are calculated to analyze the characteristics of the flow. The diagnostics are listed in Table 2 and are described below. Jet latitude is computed by fitting the zonal mean zonal wind near the jet maxima (as computed at the model's T42 resolution) to a polynomial, and then evaluating the polynomial at a meridional resolution of 0.12°. The maximum of this polynomial is the jet speed, and the latitude of this maximum is the jet latitude.

A similar polynomial best-fit procedure is followed for heat and momentum fluxes except that the fit is performed from the equator to the pole. The area-weighted heat flux is computed from 5° to 85° in order to avoid errors introduced by the polynomial fit near the endpoints. We have confirmed that this procedure is sufficient for every experiment discussed in this paper. High-frequency eddy momentum and heat flux are computed with a 7-day high-pass ninth-order Butterworth filter.

Annular mode persistence time scales are calculated as follows. An empirical orthogonal function (EOF) analysis is performed for $\sqrt{\cos\phi}$ weighted daily zonal mean zonal wind variability from 20° and poleward, pressure weighted from 100 hPa to the surface. The autocorrelation of the first principal component is computed,

TABLE 2. Summary of the diagnostics examined to analyze the characteristics of the flow and the dependence on jet location of the response to a stratospheric vortex. Here \bar{u} is a daily time series of zonally averaged zonal wind on the 300-hPa level as a function of latitude; Z_{speed} is a daily time series of maximum jet speed irrespective of latitude; Z_{latitude} is a daily time series of the latitude of this maximum jet speed; and $|\bar{V}(c)|^2$ is the power at phase speed c and latitude ϕ .

Diagnostics		
Name	Symbol	Equation
Zonal mean zonal wind	\bar{u}	
Jet latitude/speed	$Z_{\text{speed}}/Z_{\text{latitude}}$	$\max(\bar{u})$
Annular mode persistence time scale	τ	See text
High-frequency eddy momentum convergence	EMFC	$-\frac{1}{a \cos^2\phi} \left(\frac{\partial \cos^2\phi \langle \bar{u}'_{hi} v'_{hi} \rangle}{\partial \phi} \right)$
High-frequency eddy heat flux	EHF	$\frac{\langle v'_{hi} \theta'_{hi} \rangle}{\partial \theta / \partial p}$
Power-weighted average phase speed	$\bar{c}(\phi)$	$\bar{c}(\phi) = \frac{\sum_c c \bar{V}(c) ^2}{\sum_c \bar{V}(c) ^2}$

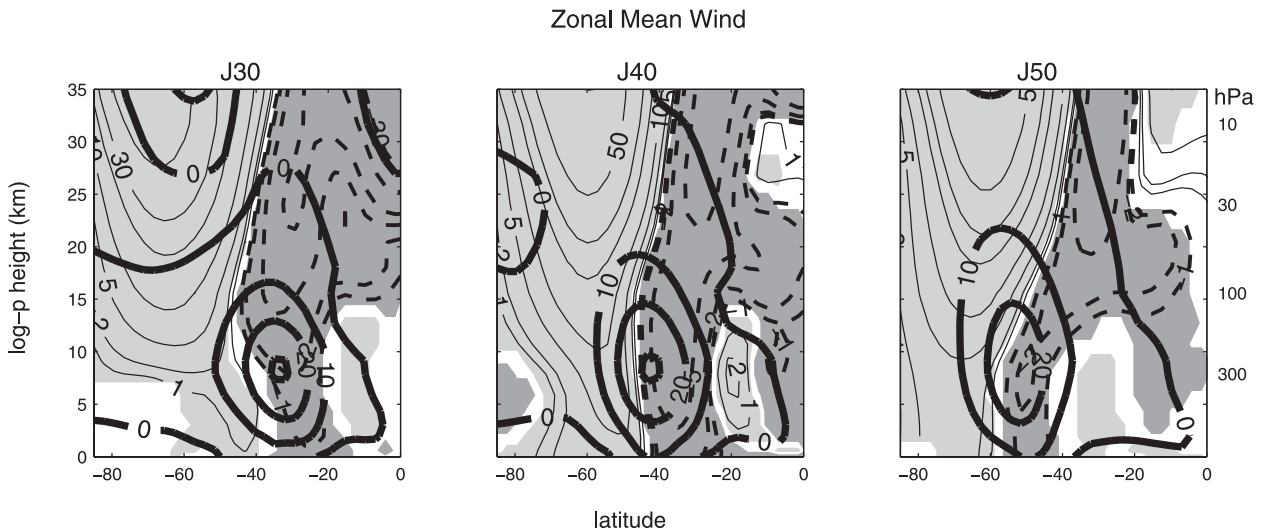


FIG. 3. Cross section of climatological zonally averaged zonal wind in the $\gamma = 0$ integrations (solid contour; contour interval 10 m s^{-1}) and the change in zonally averaged zonal wind associated with a strong vortex (thin contours and dashes shown at $\pm 1, \pm 2, \pm 5, \pm 10, \pm 20, \pm 30, \text{ and } \pm 50 \text{ m s}^{-1}$ and positive regions in light gray and negative regions in dark gray). Regions where the difference in zonal wind between the integration with a strong vortex [$\gamma = 6$ in Eq. (3)] and the integration with no vortex [$\gamma = 0$ in Eq. (3)] is statistically significant at the 95% level are shaded.

and the portion of the autocorrelation function above $1/e$ is fit to a decaying exponential. The e -folding time scale of this decaying exponential is referred to as the persistence time scale. In all cases, the first EOF dominates the zonally averaged variability.

Least squared linear best-fit lines are computed to ascertain the dependence on jet latitude of various jet properties. The uncertainty of the slope of the best-fit line is determined by the following Monte Carlo test. The jet shift, for example, in each experiment is scrambled and assigned to a random experiment. The slope of the best-fit line is then computed. Five thousand such random samples are generated, and a probability distribution function of the random best-fit slopes is constructed. The 95% uncertainty range by this Monte Carlo test is indicated.

3. An ensemble of basic states

We have created an ensemble of basic states in which jet latitude varies from 30° to 50° , and we introduce the jets in this section. The zonal mean zonal wind as a function of latitude and height for the J30, J40, and J50 cases is shown with bold lines on Fig. 3. The jet peak is around 30 m s^{-1} in all three cases and is near the latitude indicated by their names. Figure 4 shows the probability distribution function of the latitude of the daily maximum wind speed near the surface and in the upper troposphere in the J30, J40, and J50 cases. In these cases (and in all cases discussed in this paper), the distribution of daily jet latitude is unimodal and is centered around the climatological jet latitude.

In all cases, the midlatitude jet is eddy driven. We demonstrate this by comparing, in Fig. 5, the zonal wind profile at 300 hPa, heat flux at 600 hPa, and momentum flux at 300 hPa, in the J30, J40, and J50 cases. The maxima in high-frequency eddy heat flux (EHF; see Table 2) are collocated with the maxima in zonal wind (Figs. 5a–f). EHF has a similar profile in J30 and J40, and to a lesser degree in J50 (Figs. 5d–f). The maxima in high-frequency eddy momentum flux convergence (EMFC; see Table 2) for wavenumbers 4 through 13 also follow the jet maxima (Figs. 5j–l); eddies transport momentum into the jet. The correspondence between the maxima in EMFC and the jet latitude is even stronger if we consider eddies of all wavenumbers and phase speeds (not shown). In the J30 and J40 cases, eddies remove momentum from both the poleward and equatorward flanks of the jet. In contrast, in the J50 case, eddies only remove momentum from the equatorward flank [as observed for high-latitude jets by Barnes et al. (2010)].

Additional experiments with various values of A and B [see Eq. (2)] are performed to assess the robustness of the results for the J30, J40, and J50 cases (see Fig. 6). The zonal mean zonal wind peaks between 28 and 35 m s^{-1} in most cases (Fig. 6a). In the $\Delta T40$ case, peak winds are weaker because the total baroclinicity is weakened. Figures 6b and 6c compare the high-frequency EHF in the ensemble of experiments. As our methodology is to move the jet by shifting the latitude of the baroclinic region while keeping the equator-to-pole temperature difference constant, it is expected that area-weighted average upper tropospheric EHF is approximately constant in all

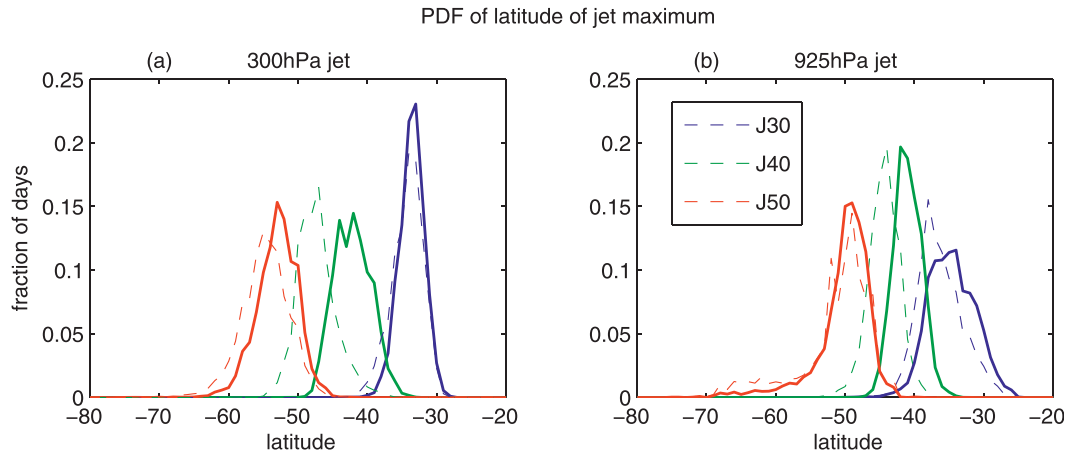


FIG. 4. Probability distribution function of jet latitude as a function of time (a) at 300 hPa and (b) at 925 hPa, in the $\gamma = 6$ (thin dashed) and $\gamma = 0$ (thick solid) integrations.

experiments (Fig. 6b). EHF is lower when the total equator-to-pole temperature difference is lowered in ΔT_{40} because tropospheric baroclinicity is reduced (denoted with a star in Fig. 6b). We do note that at lower levels (e.g., 600 hPa), the area-weighted average of high-frequency EHF does increase with jet latitude in the hemisphere with topography, although not in the hemisphere without topography (not shown). A detailed investigation of why topography might lead to increased high-frequency heat flux for higher-latitude jets is beyond the scope of this paper, but it may be related to the reduced ability of stationary eddies to advect heat poleward as the jet shifts to higher latitudes. Finally, Fig. 6c shows that the latitude of the maximum EHF shifts poleward along with jet position. The key point is that by changing tropospheric baroclinicity, we have shifted the location of the tropospheric eddy-driven jet.

4. Response to a stratospheric polar vortex

We now consider the magnitude of the shift of the midlatitude eddy-driven jet in response to changes in the stratospheric polar vortex. The light and dashed contours and shading in Fig. 3 show the change in zonal-mean zonal wind upon imposing a vortex in the J30, J40, and J50 cases. Shading indicates anomalies significant at the 95% level by a Student's t test assuming that each 100-day interval for J30 and J50, and 200-day interval for J40, is a unique degree of freedom.¹ The poleward shift of the jet

in the troposphere is present in all cases and is largest in the J40 case. The enhanced poleward jet shift is also apparent in the probability distribution function of daily jet latitude (Fig. 4). Finally, the top row of Fig. 5 confirms that the response to a vortex is strongest in the J40 case.

Figures 7a and 7b show the changes in jet latitude at 300 and 850 hPa, respectively, in the ensemble of experiments. The poleward jet shift is largest for jets near 40° in both the upper and lower troposphere, whereby the overall pattern resembles an inverted V (hereafter called a chevron). The slope between 40° and 50° is similar to that in Kidston and Gerber (2010) and Barnes and Hartmann (2010), who considered the response of the SH tropospheric jet to increased CO₂ (among other changes) in an ensemble of GCMs, and the difference between jets at 40° and 30° is similar to the difference between the Pacific and Atlantic sector responses in the reanalysis, as noted in section 1. Hence, the dry model appears to capture the relationship between the response of a jet to external forcing and jet latitude that is found in observations and more comprehensive models.

One might argue that the response in J30 is weaker because the jet is farther away from the polar vortex. We therefore explore the sensitivity of the tropospheric response to vortex width. Three additional 5100-day experiments are performed that are identical to J30, J40, and J50, respectively, except that the anomalous vortex cooling extends farther equatorward [ϕ_0 in Eq. (4) is set to 40° rather than 50°]. Even for the broader cooling, the effect of a vortex on tropospheric jet latitude is still much larger for a jet at 40° than for a jet at 30° (see Fig. 7c).

Finally, we have explored sensitivity to model resolution. Three additional 5100-day experiments are performed that are identical to J30, J40, and J50, respectively, except that the resolution is T63 as opposed to T42. At the higher

¹ Further analysis is needed to better quantify the appropriate degrees of freedom for this sGCM configuration, but these intervals exceed the annular mode persistence time scale in all cases (to be discussed later) and are likely a conservative estimate on the true number of degrees of freedom in the troposphere.

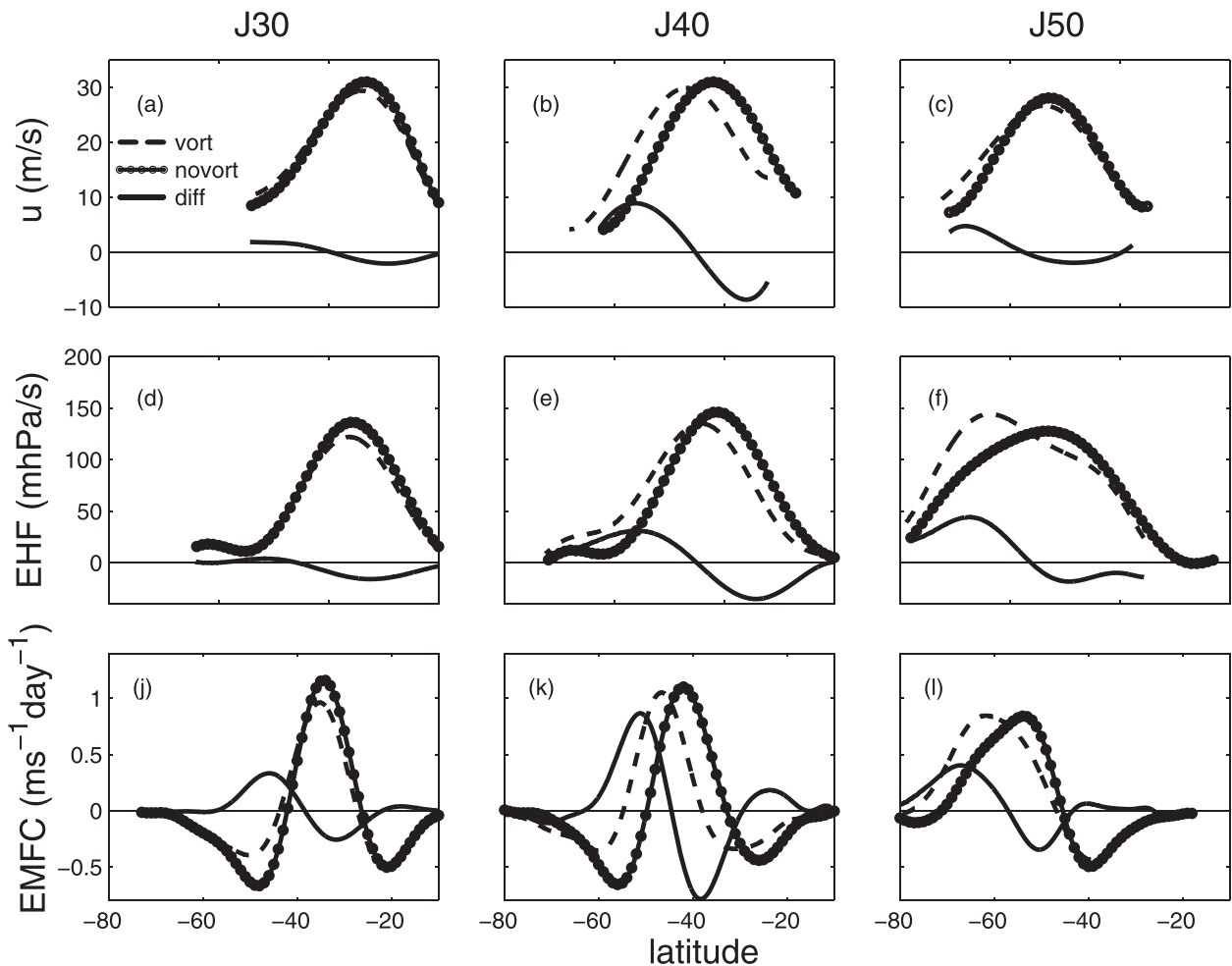


FIG. 5. Zonal wind at 300 hPa in m s^{-1} , high-frequency eddy heat flux (EHF) at 600 hPa in m hPa s^{-1} , and high-frequency synoptic eddy momentum flux convergence (EMFC) at 300 hPa in $\text{m s}^{-1} \text{ day}^{-1}$, in the J30, J40, and J50 cases. The $\gamma = 0$ integration is represented by a circle–solid line, and the $\gamma = 6$ integration is represented by a dashed line.

resolution, the effect of a vortex on tropospheric jet latitude is still larger for a jet at 40° than for a jet at 30° or 50° , although differences are weaker (see Fig. 7d). As discussed in section 6, the change in sensitivity is consistent with a change in the tropospheric eddy feedback with resolution.

The shift in zonal mean winds is associated with changes in synoptic eddy momentum fluxes (as in Kushner and Polvani 2004, their Fig. 8b). Anomalies of EMFC develop in response to the vortex, whereby eddies accelerate the jet poleward and decelerate the jet equatorward of its position in the control integration (solid line in Figs. 5j–l). The difference between the maxima and minima of the anomalous EMFC is taken for each case and is shown in Fig. 7e. Anomalous EMFC, like the change in jet latitude, resembles a chevron. If we focus on synoptic wavenumber and high-frequency EMFC only (Fig. 7f), the chevron is even clearer. As vertically

averaged ($\partial \overline{u'v'}/\partial y$) must balance surface friction for a steady-state surface jet, for example, Held (1975) and section 12.1 of Vallis (2006), it is therefore to be expected that changes in EMFC are consistent with the magnitude of the shift of the eddy-driven jet. [Figure 11a shows that the magnitude of the jet shift follows qualitatively the change in EMFC. The rest of this study seeks to explain why the shift of the jet (or equivalently, the change in eddy momentum flux) is larger for a jet at 40° than for a jet at 30° or 50° .]

5. A quantitative assessment of mechanisms for a jet shift

Several recent studies have proposed mechanisms for how external variability can modify jet latitude. Here we examine whether these mechanisms are

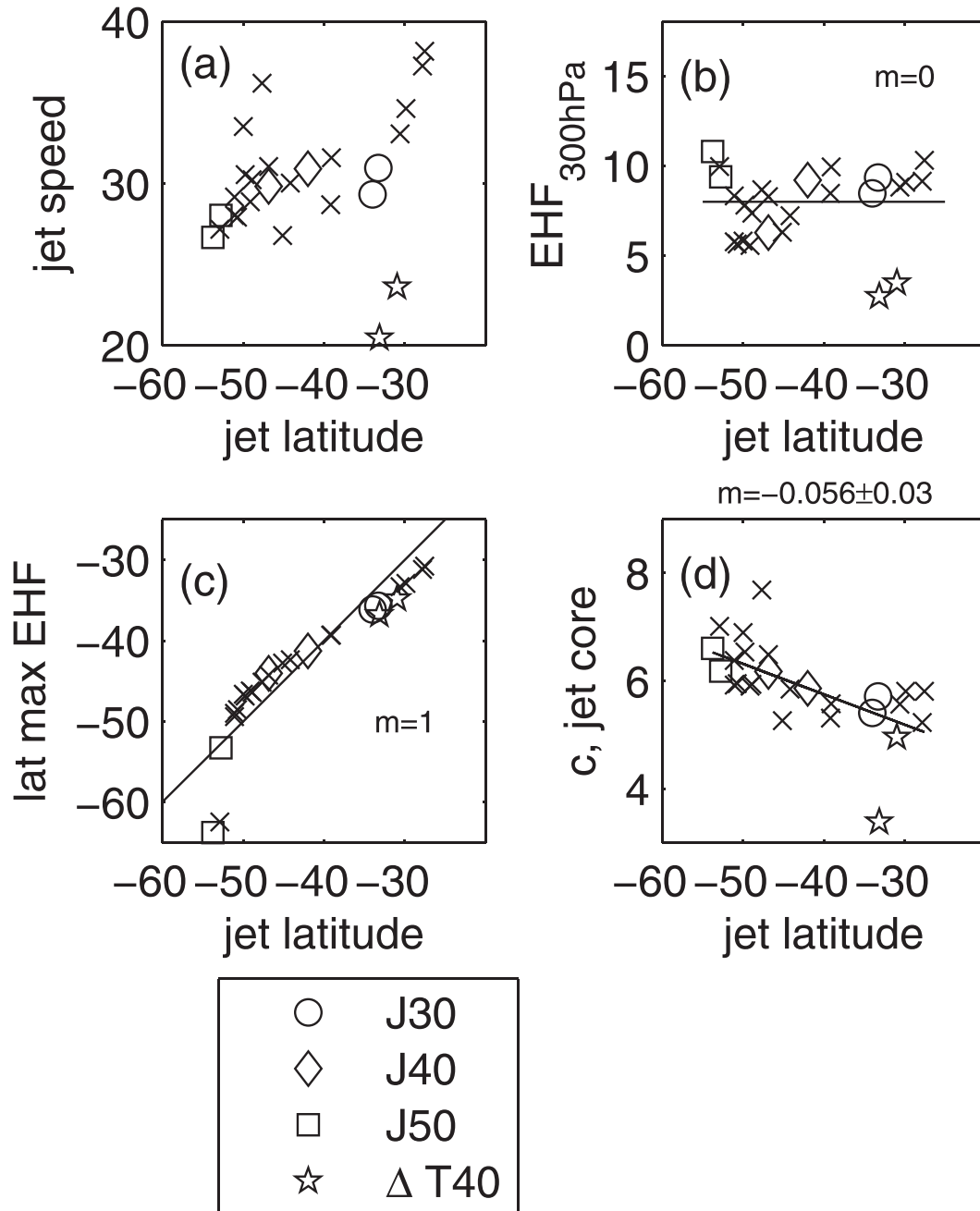


FIG. 6. Scatterplots of jet and eddy behavior as a function of jet latitude and tropospheric forcing. (a) Peak zonal wind speed (m s^{-1}) below 150 hPa. (b) Area-weighted high-frequency eddy heat flux (m hPa s^{-1}) at 300 hPa. (c) Latitude of the maximum EHF at 600 hPa. (d) Power-weighted eddy phase speed at the jet core (m s^{-1}). On (b) a line with zero slope is drawn; on (c), a line indicating a one-to-one relationship is drawn; and on (d), a best-fit line is drawn and the slope and uncertainty is indicated. Each marker represents one sGCM integration. Special markers denote the J30, J40, J50, and $\Delta T40$ integrations, while all other integrations are denoted with an x, in this figure and all future similar figures.

consistent with the relationship between jet latitude and the response to the polar vortex. In particular, can changes in eddy phase speed, eddy heat flux, eddy zonal length scale, lower stratospheric index of

refraction, stratospheric PV inversion, and/or planetary waves explain the dependence on tropospheric jet latitude of the jet's response to stratospheric perturbations?

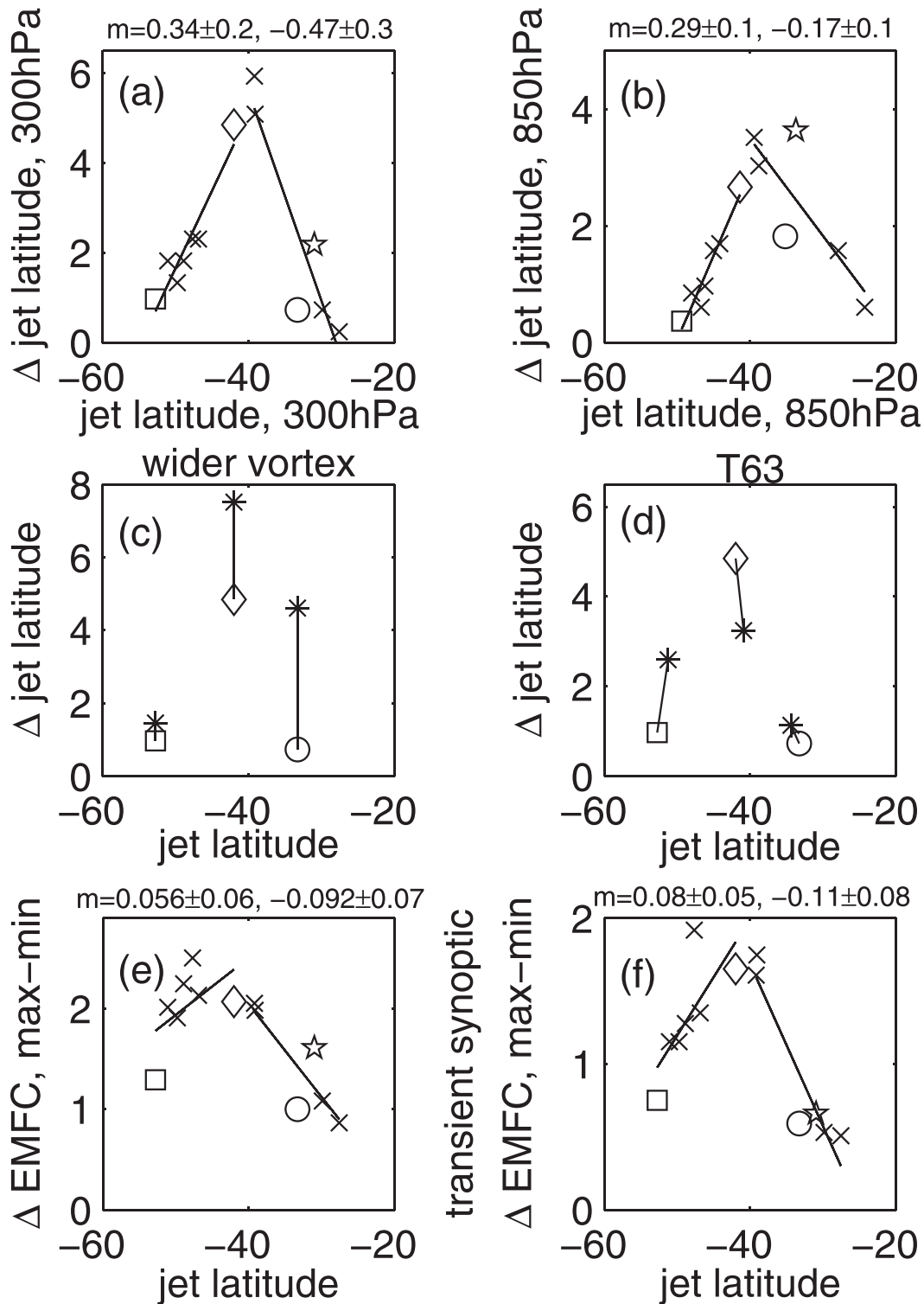


FIG. 7. Scatterplots of the difference in jet and eddy behavior between the strong polar vortex integration and no polar vortex integration. (a) Poleward shift in jet latitude at 300 hPa. (b) Poleward shift in jet latitude at 850 hPa. (c) Poleward shift in jet latitude at 300 hPa for a vortex width of 50° and 40° (in all cases, the larger jet shift occurs for a vortex width of 40° , denoted with asterisks). (d) Poleward shift in jet latitude at 300 hPa for T63 and T42 integrations (asterisks denote T63). (e) Difference in eddy momentum flux convergence, all wavenumbers and frequencies, in $\text{m s}^{-1} \text{ day}^{-1}$ between largest positive and negative anomalies (i.e., max - min of the solid curves on Figs. 5g-i) at 300 hPa. (f) As in (e), but for wavenumbers 4 to 13 and high frequencies only. Best-fit lines are included on (a),(b),(e), and (f) with the fit performed separately for jets equatorward and poleward of 40° . The slope of the line and the uncertainty is shown.

a. Eddy phase speed

A potential mechanism to explain stratosphere–troposphere coupling is that increased lower stratospheric winds cause eddy phase speeds to increase, which then impacts the location of critical lines and thus wave convergence, and subsequently causes a poleward shift (Chen and Held 2007). To test this, the difference in power-weighted eddy phase speed calculated at the latitude of the jet maxima [$\bar{c}(\phi_{\text{jetmax}})$] is shown in Fig. 8a. We find no systematic change in the phase speeds, and certainly no evidence that the perturbations resemble the chevron structure of the response. Results are not sensitive to the use of angular phase speed as opposed to phase speed, or vorticity as opposed to EMFC, when computing $\bar{c}(\phi_{\text{jetmax}})$. Because we do not find an increase in tropospheric wind speed in response to a stronger vortex (Figs. 5a–c and 6a), our results are not contradictory to those of Chen and Held (2007). However, wind speeds do increase poleward of the jet core in our experiments. We therefore show the changes in eddy phase speed poleward of the jet core in Fig. 8b. Although phase speeds do increase in most cases (and especially for more poleward jets, as in the Southern Hemisphere), we still do not find a chevron pattern. Changes in eddy phase speed cannot simply explain the dependence of the response on the climatological jet location.

b. Eddy heat fluxes

Thompson and Birner (2012) highlight the importance of upper tropospheric baroclinicity for the tropospheric response to polar vortex anomalies, and anomalies in EHF develop in response to including a vortex in our experiments (solid line in Figs. 5d–f). To test whether heat flux anomalies might be leading to the chevron-shaped response in our experiments, we evaluate the difference between the maxima and minima of the anomalous EHF for each case and show it in Fig. 8c. Changes in EHF do not resemble the chevron pattern of the magnitude of the jet shift. Changes in EHF higher in the troposphere look qualitatively like those at 600 hPa (cf. Figs. 8c and 8d). We thus conclude that while EHF does change in response to a vortex, as in Thompson and Birner (2012), changes in EHF do not appear to be correlated with changes in the magnitude of the jet shift in our experiments. Note that Simpson et al. (2012) also conclude that changes in EHF are not consistent with the magnitude of the jet shift in their transient experiments.

c. Eddy length scale

Kidston et al. (2010) find that eddy length scales have increased in the SH over the past three decades, and

Rivière (2011) argues that such a change could lead to a poleward shift in the jet. While the precise mechanism whereby increased eddy length scales can lead to a poleward shift in the jet differs between these authors, polar vortex variability can influence upper tropospheric baroclinicity directly, and Rivière (2011) argues that a change in upper-level baroclinicity changes eddy length scales. To test whether this effect might explain the magnitude of the poleward shift in our experiments, we examine the change in zonal eddy length scale for vorticity at the jet core [computed as in Barnes and Hartmann (2011)]. While the eddy length scales increase in response to the poleward shift (Fig. 8e), the intra-ensemble pattern does not resemble a chevron and is not consistent with the variability with jet latitude of the magnitude of the jet shift. Results are similar if we compute the eddy length scale on either flank of the jet or averaged over the midlatitudes (not shown).

d. Planetary waves

A potential mechanism to explain stratosphere–troposphere coupling is that vertical and meridional gradients of zonal wind in the stratosphere reflect planetary waves back into the troposphere, where they couple with the tropospheric planetary waves and subsequently modify the zonal mean flow (Perlwitz and Harnik 2003; Shaw et al. 2010). To test whether planetary waves contribute to the jet shift, we have examined the wavenumbers responsible for the tropospheric response. We find that transient waves of synoptic wavenumbers, and not planetary wavenumbers, are the dominant contributor to the chevron pattern (not shown, but most of the chevron in Fig. 7e is captured by Fig. 7f). Nevertheless, we do find changes in high-latitude planetary waves (i.e., poleward of 60°) in response to a vortex (as in Sun et al. 2011). In particular, we find that planetary waves act to decrease the poleward jet shift for J40 and increase it for J50 (for J30, their effect is too far poleward of the jet core to have any impact), which is opposite to the observed chevron pattern. Furthermore, the polar vortex imposed in the J30, J40, and J50 cases is identical, and so the resulting vertical and meridional gradients are nearly identical as well. A wave reflection mechanism does not appear to simply explain the relationship between jet latitude and the magnitude of the jet shift.

e. Stratospheric PV inversion

A potential mechanism to explain stratosphere–troposphere coupling is that an axisymmetric circulation must develop in order to maintain thermal wind balance with anomalies in the polar vortex, and this axisymmetric circulation extends into the troposphere (Ambaum and Hoskins 2002). To test this, axisymmetric modeling

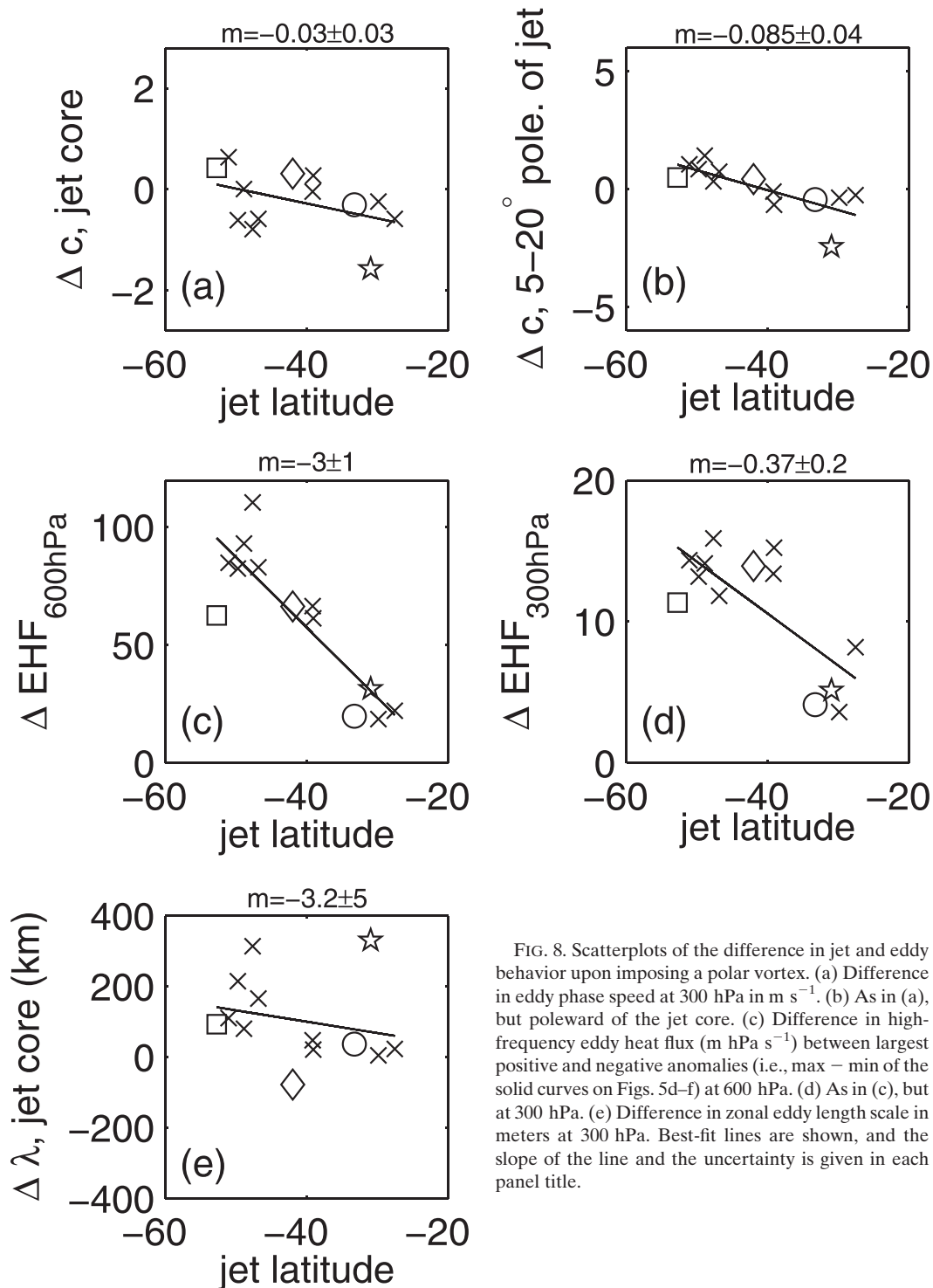


FIG. 8. Scatterplots of the difference in jet and eddy behavior upon imposing a polar vortex. (a) Difference in eddy phase speed at 300 hPa in m s^{-1} . (b) As in (a), but poleward of the jet core. (c) Difference in high-frequency eddy heat flux (m hPa s^{-1}) between largest positive and negative anomalies (i.e., $\text{max} - \text{min}$ of the solid curves on Figs. 5d–f) at 600 hPa. (d) As in (c), but at 300 hPa. (e) Difference in zonal eddy length scale in meters at 300 hPa. Best-fit lines are shown, and the slope of the line and the uncertainty is given in each panel title.

integrations have been performed for the J30, J40, and J50 cases and the anomalous circulation in the troposphere due to a vortex compared among the three cases. The axisymmetric circulation is essentially identical in all cases (Figs. 9a,b). The balanced response to PV

anomalies in the stratospheric vortex cannot simply explain the magnitude of the jet shift associated with vortex anomalies. Song and Robinson (2004), Kushner and Polvani (2004), and Son et al. (2010) all reach a similar conclusion.

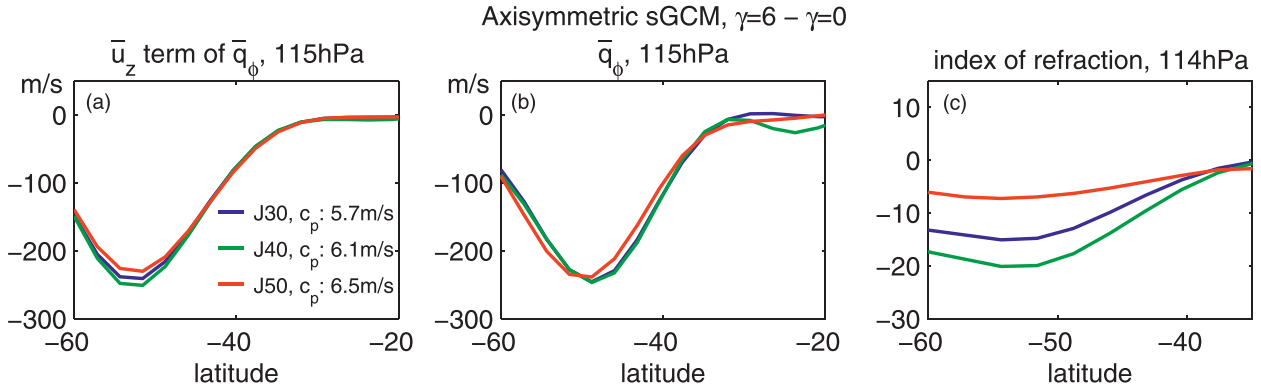


FIG. 9. Axisymmetric circulation in response to a vortex in the J30, J40, and J50 cases: (a) $[(\rho_0 f^2/N^2)(\partial u/\partial z)]_z$ multiplied by Earth's radius, (b) the meridional gradient of potential vorticity (\bar{q}_ϕ multiplied by Earth's radius), and (c) the index of refraction multiplied by Earth's radius. Note that the abscissa of (c) differs from (a) and (b); (a) and (b) have units of m s^{-1} and (c) is unitless.

f. Stratospheric index of refraction

Chen and Robinson (1992), Limpasuvan and Hartmann (2000), and Hartmann et al. (2000) argue that the quigeostrophic index of refraction can be used to diagnose the preferred direction of Rossby wave propagation in response to anomalies in the stratospheric polar vortex. According to linear theory, waves tend to propagate within regions of positive index of refraction and propagate toward regions with a larger index of refraction. The index of refraction can be written as

$$n_s^2 = \frac{\bar{q}_\phi}{a(\bar{u} - c)} - \frac{s^2}{a^2 \cos^2 \phi} - \frac{f^2}{4N^2 H^2} \quad \text{and}$$

$$\bar{q}_\phi = 2\Omega \cos \phi - \frac{(\bar{u} \cos \phi)_\phi}{a \cos \phi} - \frac{a}{\rho_0} \left(\frac{\rho_0 f^2 \partial u}{N^2 \partial z} \right)_z, \quad (5)$$

where we use the same notation as on p. 240 of Andrews et al. (1987), and c is the eddy phase speed. To analyze whether this effect might explain the magnitude of the jet shift, axisymmetric integrations with and without a vortex for the J30, J40, and J50 cases are performed. A colder polar vortex leads to decreased static stability and a larger $\partial u/\partial z$ in the lower stratosphere. Both of these effects lead to larger $[(\rho_0 f^2/N^2)(\partial u/\partial z)]_z$ (Fig. 9a) and decreased \bar{q}_ϕ (Fig. 9b). The index of refraction is then computed for waves with the power-weighted eddy phase speed of the corresponding nonaxisymmetric integration (shown in Fig. 6e). A colder polar vortex leads to lower index of refraction values over the subpolar lower stratosphere (Fig. 9c). Because the index of refraction decreases poleward of the jet maximum, equatorward propagation of eddies and poleward momentum flux is enhanced, leading to a poleward shift in the jet.

We now consider differences in this effect among the J30, J40, and J50 experiments. In the J40 case, this effect

is strongest (cf. Fig. 9c). The strengthening of the effect for J40, however, is not due to any differences in the axisymmetric circulation forced by the vortex, as Figs. 9a and 9b suggest that the circulation is nearly identical in all cases. Rather, the effect is mainly due to the power-weighted eddy phase speed and nonlinearities within the index of refraction calculation (not shown). While this effect is consistent with the weaker response in J30 and J50 than in J40, it is difficult to quantify the contribution of this effect to the difference in tropospheric responses, as the effect is very sensitive to the precise phase speed used when calculating the index of refraction.

g. Summary

We have shown that changes in eddy phase speed, eddy heat flux, eddy zonal length scale, lower stratospheric index of refraction, stratospheric PV inversion, and planetary waves cannot simply explain, even qualitatively, why the J40 jet should be more sensitive than the J30 or J50 jets (with the possible exception of lower stratospheric index of refraction). While this does not necessarily disprove any of them, it does confirm that these mechanisms alone cannot explain the magnitude of the tropospheric response to a stratospheric perturbation. We therefore turn to a *tropospheric* mechanism that focuses on internal jet variability in order to explain the magnitude of the tropospheric response.

6. The role of natural variability and eddy feedback in the magnitude of the response

Ring and Plumb (2007) and Gerber et al. (2008) find that changes in the magnitude of a jet shift qualitatively follow the annular mode persistence time scale. We therefore examine whether jet persistence, and thus the response to a vortex, might be enhanced for a jet near

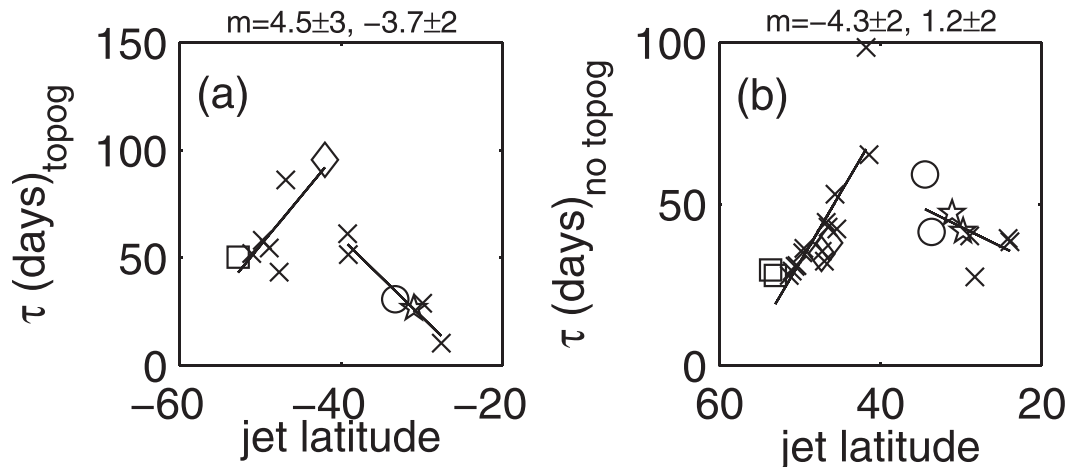


FIG. 10. Scatterplots of jet and eddy persistence as a function of jet latitude and tropospheric forcing. (a) Persistence time scale of the first EOF. (b) Persistence time scale of the first EOF in the hemisphere without topography. For (a), we show only the integration with $\gamma = 0$ (so that there is no stratosphere–troposphere coupling on intraseasonal time scales), while for (b) we show all integrations (note that the polar vortex is imposed in the hemisphere with topography only). Best-fit lines are included on all plots, with the fit performed separately for jets equatorward and poleward of 40°. The slope of the line and the uncertainty is shown.

40°. Figure 10 compares jet latitude and jet persistence. Figure 10a shows the annular mode time scale for each model integration. Deviations of the annular mode persist the longest for a jet near 40°, with a chevron describing the persistence for jets farther equatorward or poleward. Figure 10b shows that annular mode time scales resemble a chevron even in the hemisphere without topography. A discontinuity exists near 40° in the hemisphere with topography. This kink exists even if we look at upper or lower tropospheric persistence time scale or time scales on various sigma levels. Future work is needed to better understand the nature of this kink and its potential relationship with the regime behavior in Wang et al. (2012). Note that some of the weakening of the effect for a jet near 40° for T63 resolution relative to T42 resolution (Fig. 7d) can be attributed to changes in the annual mode persistence time scale (which is reduced at T63 resolution; not shown). Finally, Fig. 11b shows that the magnitude of the jet shift follows qualitatively the annular mode persistence time scale (as in Gerber et al. 2008). However, we note that there is more scatter than for EMFC (Fig. 11a).

We do not mean to argue that the annular mode time scale itself fully explains the increased response of the J40 jet to the stratospheric perturbation. Rather, it serves as an effective way to quantify the feedback strength between eddies and the zonal mean flow (Gerber and Vallis 2007). We note that this correspondence between annular mode persistence and eddy feedback fails when the surface friction is modified (Chen and Plumb 2009). However, the surface friction is held constant in our

integrations, and we find that the annular mode time scale well quantifies the strength of the feedback, as computed with the analysis of Lorenz and Hartmann (2001). See the appendix for additional details.

Fluctuation–dissipation theory (Leith 1975) suggests that the magnitude of the response of a mode to a given forcing will depend not only on the time scale of the observed fluctuations, but also on the projection of the forcing on the mode. It is difficult to quantify the projection onto the mode from these experiments, however, as the projection likely depends on which specific stratosphere–troposphere coupling mechanism discussed in section 5 one deems most important. However, we have performed experiments with a wider vortex (cf. Fig. 7c), and we find that even for the broader cooling, the effect of a vortex on tropospheric jet latitude is still much larger for a jet at 40° than for a jet at 30°. Overall, our results indicate that the strength of tropospheric feedbacks is consistent with the chevron pattern for the magnitude of the jet shift.

Chan and Plumb (2009) and Gerber and Polvani (2009) note regime behavior and bimodality of the jet in the presence of a vortex for jets near 40° in sGCM simulations, and regime behavior can substantially impact jet persistence (and magnify the response to a vortex; e.g., PK02). However, we have confirmed that regime behavior is not responsible for the enhanced persistence of our J40 case. Figure 4 shows that the distribution of daily jet latitude is unimodal in our experiments in both the $\gamma = 0$ and $\gamma = 6$ integrations. In the J30 and J50 cases, there is a tail toward higher jet latitudes near the surface,

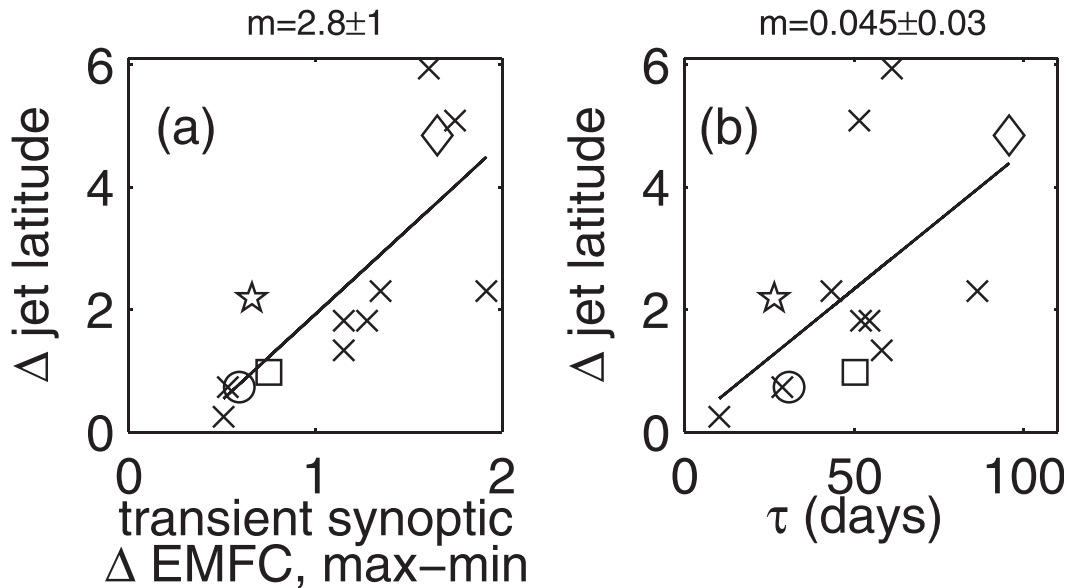


FIG. 11. Scatterplots of jet and eddy behavior in response to a polar vortex. (a) Relationship between the EMFC (in $\text{m s}^{-1} \text{day}^{-1}$) and the change in jet latitude at 300 hPa (b) Relationship between the persistence time scale of the first EOF (in days) and the change in jet latitude at 300 hPa. Best-fit lines are included on all plots, and the slope of the line and the uncertainty are shown.

and such a feature might suggest the presence of regimes (e.g., Wang et al. 2012). However, this feature is absent in our J40 integration, which has the most persistent variability. Annual mode persistence time scales are below 140 days in all experiments as well. Note that in the presence of topography, as in our experiments, jet bimodality is substantially weakened (e.g., Gerber and Polvani 2009). Our jets do not demonstrate regime-like behavior and thus the enhanced persistence for J40 is dynamically meaningful. In summary, *tropospheric* synoptic eddy dynamics appear to dominate the quantitative structure of the response.

7. Conclusions

A dry primitive equation model is used to show that the tropospheric response to a stratospheric polar vortex is strongest for a jet centered near 40° and weaker for jets near 30° and 50° . This result suggests that part of the difference between the North Pacific and North Atlantic in the response to NH stratospheric polar vortex anomalies is due to the difference in jet latitude. In addition, jet latitude can explain some of the intramodel variability in the magnitude of the trend in the SH over the past 30 years.

The likely cause of the enhanced tropospheric response for a jet centered near 40° is the stronger tropospheric eddy feedback present in a jet located near 40° . In contrast, eddy phase speed, eddy heat flux, stratospheric PV inversion, planetary wave, and eddy zonal length scale

arguments do not appear to be capable of simply explaining this effect.

We note that even if the stratospheric-focused mechanisms cannot explain the magnitude of the shift, they might still be valid for understanding the initial impact of the stratosphere on the tropospheric jet, which in turn is amplified by eddy-mean flow interactions in the troposphere. The net effect, however, is that the amplitude of the response to polar stratospheric cooling depends strongly on eddy-zonal flow tropospheric feedbacks. This might explain why it is extremely hard to “prove” any specific mechanism in equilibrated or transient simulations: the evidence supporting each mechanism is likely buried under these massive tropospheric feedbacks. We therefore suggest that future work should utilize models where tropospheric feedbacks are explicitly suppressed in order to make progress on the mechanisms that couple the troposphere and stratosphere [e.g., the shallow water model in Chen et al. (2007)].

Finally, we suggest that changes in eddy phase speed, eddy zonal length scale, and EHF cannot explain the magnitude of the trend in the SH circulation over the past 30 years. Rather, our results suggest that these three effects might be a consequence or a by-product of a poleward shifting jet, as all three of these tend to increase or shift poleward as jets shift poleward, even in the absence of any stratospheric forcing. For example, Barnes and Hartmann (2011) show systematic changes in eddy length scale when the jet is shifted poleward, and Figs. 6c and 6d show similar systematic changes for heat

flux and phase speed. In contrast, changes in eddy feedback can explain the magnitude of the shift.

The sensitivity of the response to the mean state of the unperturbed climate highlights the complexities in the atmospheric system. While a dry model has fundamental limitations on its ability to simulate the actual atmosphere, it is remarkable that a relatively simple model like the one used here is capable of qualitatively capturing the observed signal.

Acknowledgments. This work was supported by the NASA Grant NNX06AE70G and NSF Grants ATM 0905863 and AGS 0938325. We acknowledge NCAR's Computational and Information Systems Laboratory for providing computing resources. We thank the anonymous reviewers for their comments and G. Chen for advice on cospectra calculations.

APPENDIX

Natural Variability

In this appendix, we confirm that the annular mode time scale is a valid metric of eddy feedback strength. We then show that the chevron-shaped pattern of annular mode time scale is consistent with previous work on the relative contribution of jet shifts and pulses to total jet variability.

As the annular mode is a highly derived quantity, we first verify that it captures the persistence of the flow by examining two kinematic metrics of jet persistence. The number of days between the start of a poleward shifted jet event (calculated as the first day in which jet latitude exceeds 10% of its natural variability) and the end of a poleward shifted jet event (calculated as the first day after the start of a poleward shifted event in which jet latitude drops below 33% of its natural variability) is computed and the average duration is shown in Fig. A1a. Poleward shifted jet events last longer for jets centered near 40°. The chevron shape is robust to changing the thresholds for the start and end of a poleward shifted jet event. Figure A1b is equivalent to Fig. A1a but for equatorward shifted jets; although there is more scatter than for poleward shifted jets, equatorward shifted jet events last longer for jets centered near 40° as well. Jets centered near 40° have more persistent variability in our sGCM experiments.

Lorenz and Hartmann (2001) and Eichelberger and Hartmann (2007) show that eddies, and in particular high-frequency EMFC, positively feed back on the shifting of the jet that is associated with deviations of the annular mode. Specifically, the eddy momentum flux convergence shifts as the jet shifts in such a way as to

provide a positive feedback on jet latitude. Figure A2a shows the lagged correlation between the forcing time series by high-frequency EMFC of annular mode deviations and the principal component time series of the annular mode [computed as in Lorenz and Hartmann (2001) and Eichelberger and Hartmann (2007), except that we pressure-weight the EMFC anomalies only down to 500 hPa to avoid complications due to the topography]. At lag 0, EMFC anomalies are driving the annular mode anomaly in all cases. At positive lags, however, the correlation between the EMFC forcing and the annular mode anomaly time series is still high, implying a positive eddy feedback (Lorenz and Hartmann 2001), in all cases. The positive correlation at large positive lags is strongest for J40; hence, eddy feedback by momentum fluxes is strongest for J40 as well. Enhanced eddy feedback in J40 implies that the persistence time scale will be larger. Figure A2b is equivalent to Fig. A2a except that we use the time series of *jet latitude* and the projection of the high-frequency EMFC on the spatial pattern associated with a change in *jet latitude*. It is clear that EMFC anomalies act to maintain a change in jet latitude well after the shift in jet latitude has occurred. This effect is summarized in Fig. A1c, which shows the average lagged correlation from day 8 to day 88 after an annular mode event. Figure A1d is similar, but it shows the average lagged correlation from day 8 to day 88 after a jet shift. The eddy feedback of annular mode anomalies and of jet shift anomalies resembles a chevron in our sGCM ensemble. As the jet approaches either the subtropics or the pole, eddy feedback becomes weaker.

Furthermore, the relative importance of shifting of the jet for the total variability of the jet differs among the experiments, as in the barotropic model experiments of Barnes and Hartmann (2011). Figures A1e and A1f show the relative role of jet speed and jet latitude in the total variability of the jets in our sGCM ensemble. The variance of the jet associated with jet speed is defined as $\text{frac}_{\text{speed}} = \{\sum_{\text{eq.}}^{\text{pole}} \text{CS}^2[\text{var}_{\text{time}}(\bar{u})]\} / \{\sum_{\text{eq.}}^{\text{pole}} \text{var}_{\text{time}}(\bar{u})\}$, and the variance of the jet associated with jet latitude is defined as $\text{frac}_{\text{latitude}} = \{\sum_{\text{eq.}}^{\text{pole}} \text{CL}^2[\text{var}_{\text{time}}(\bar{u})]\} / \{\sum_{\text{eq.}}^{\text{pole}} \text{var}_{\text{time}}(\bar{u})\}$, where \bar{u} is a daily time series of zonally averaged zonal wind on the 300-hPa level as a function of latitude, $\text{var}_{\text{time}}(\bar{u})$ is the temporal variance of zonal wind at a given latitude, and $\text{CS}(\text{lat}) = r[Z_{\text{speed}}, \bar{u}(\text{lat})]$ is the temporal correlation between Z_{speed} and zonal wind at each latitude—CL is similar: $\text{CL}(\text{lat}) = r[Z_{\text{latitude}}, \bar{u}(\text{lat})]$ —where Z_{speed} is a daily time series of maximum jet speed irrespective of latitude and Z_{latitude} is a daily time series of the latitude of this maximum jet speed. Figures A1e,f show that more of the variance of a jet near 40° is associated with jet latitude as compared to jet speed. In contrast, an increasing

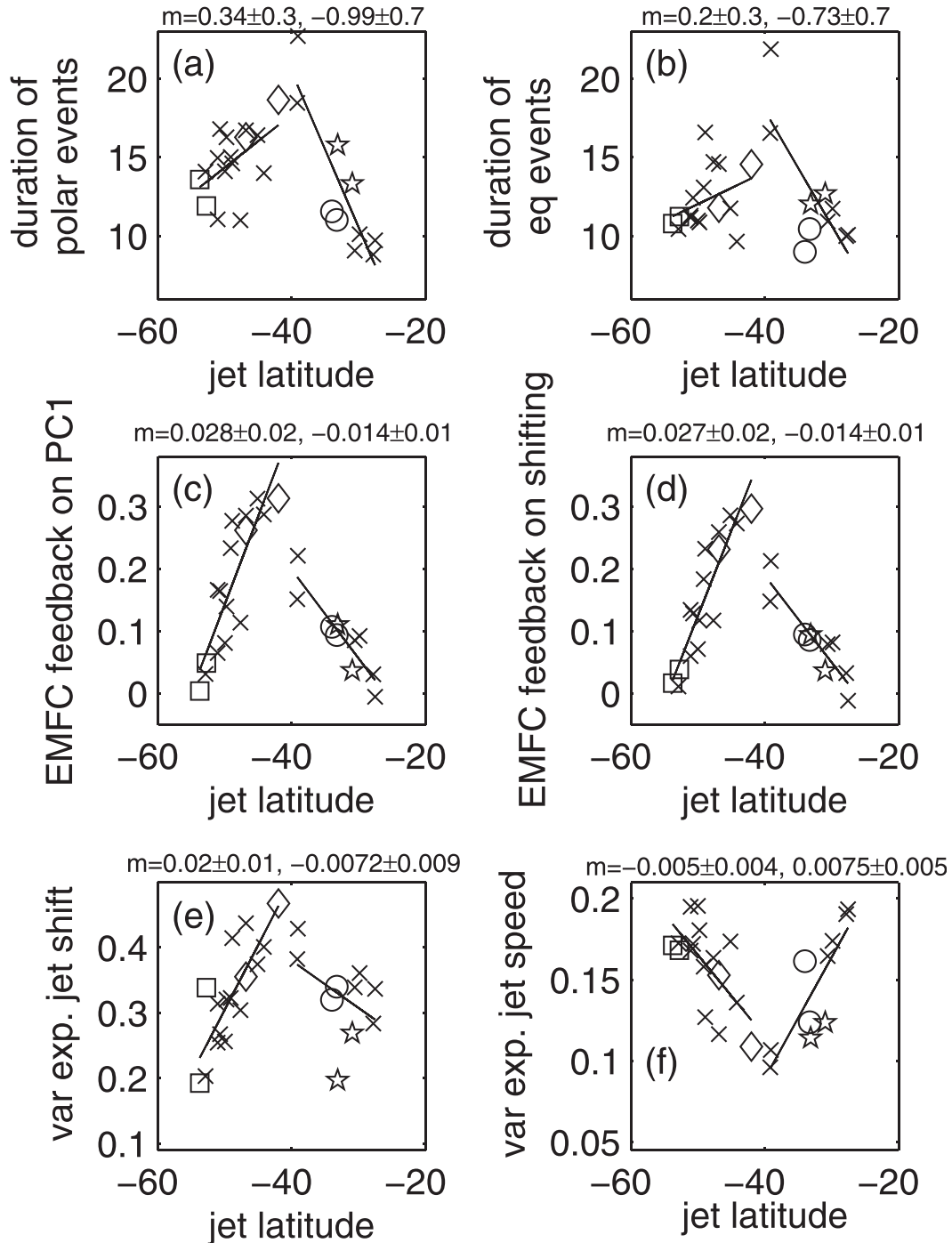


FIG. A1. Scatterplots of jet and eddy persistence as a function of jet latitude and tropospheric forcing. (a) Average duration of poleward shifted jet events at 300 hPa (see text for details). (b) Average duration of equatorward shifted jet events at 300 hPa (see text for details). (c) Average lagged correlation from 8 to 88 days between the high-frequency EMFC forcing time series associated with the annular mode and the time series of the annular mode. (d) As in (c), but for jet shifting instead of the annular mode. (e) Fraction of variance of the jet at 300 hPa associated with jet shifting (see text for details). (f) Fraction of variance of the jet at 300 hPa associated with jet speed (see text for details). Best-fit lines are included on all plots, with the fit performed separately for jets equatorward and poleward of 40° . The slope of the line and the uncertainty is shown. For all panels, we focus on the hemisphere with topography.

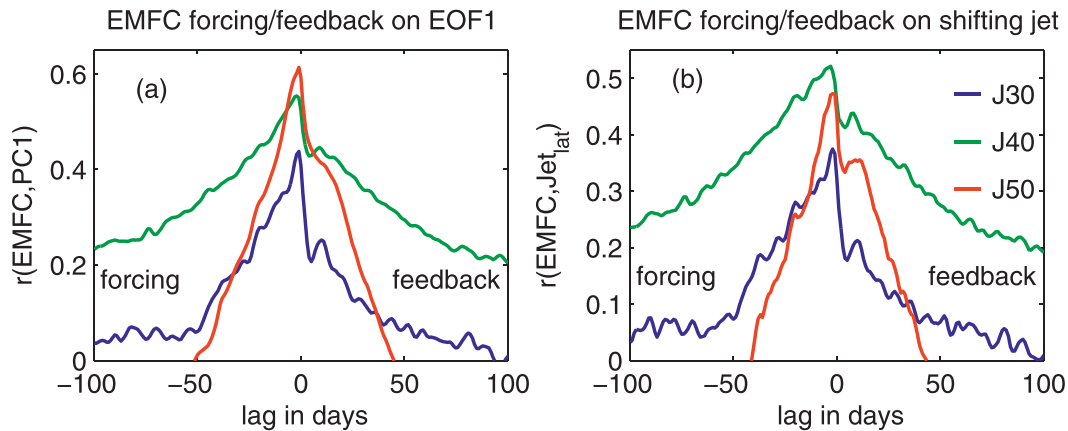


FIG. A2. Forcing and feedback of jet shifts and annular mode deviations by eddy fluxes. High correlations indicate that eddies are acting to create (for negative lags) and maintain (for positive lags) a jet shift or pulse. (a) Lagged correlation between the time series of the annular mode and the time series of the projection of the high-frequency EMFC pattern associated with a deviation of the annular mode onto the daily EMFC. (b) Lagged correlation between the time series of jet latitude and the projection of the high-frequency EMFC pattern associated with a shifting of the jet onto the daily high-frequency EMFC. For (a) and (b), the EMFC is pressure weighted and then vertically averaged.

share of the variance of a jet near 30° or 50° is associated with jet speed. Both of these effects are also apparent in the barotropic model experiments of Barnes and Hartmann (2011). Note that even for jets near 30° or 50° , most of the variability is associated with shifting (and thus examining a latitude–height cross section of the zonal wind anomalies associated with annular mode anomalies is not revealing); the relative ratio of shifting to pulsing appears to be the important criterion. As the jet approaches either the subtropics or the pole, pulsing becomes relatively more important and shifting becomes relatively less important in explaining jet variability. Since previous work suggests that shifts of the jet are more persistent than pulses of the jet (Lorenz and Hartmann 2001; Robinson 2006; Eichelberger and Hartmann 2007; Barnes and Hartmann 2011), it is to be expected that annular mode time scales are largest for jets near 40° in our sGCM experiments.

In summary, differences in eddy feedback strength, and in the relative importance of pulsing versus shifting in describing total jet variability, appear to dictate the strength of the response of EMFC, and thus of the jet itself, to external forcing. As jet variability for jets near 40° appears to be associated more with shifting than pulsing, jets near 40° appear to have more persistent variability and a stronger response to the vortex.

REFERENCES

- Ambaum, M. H. P., and B. J. Hoskins, 2002: The NAO troposphere–stratosphere connection. *J. Climate*, **15**, 1969–1978.
- Andrews, D. G., J. R. Holton, and C. B. Leovy, 1987: *Middle Atmosphere Dynamics*. Academic Press, 489 pp.
- Arblaster, J. M., and G. A. Meehl, 2006: Contributions of external forcings to southern annular mode trends. *J. Climate*, **19**, 2896–2905.
- Baldwin, M. P., and T. J. Dunkerton, 1999: Propagation of the Arctic Oscillation from the stratosphere to the troposphere. *J. Geophys. Res.*, **104** (D24), 30 937–30 946.
- , and —, 2001: Stratospheric harbingers of anomalous weather regimes. *Science*, **294**, 581–584.
- , D. B. Stephenson, D. W. J. Thompson, T. J. Dunkerton, A. J. Charlton, and A. O'Neill, 2003: Stratospheric memory and skill of extended-range weather forecasts. *Science*, **301**, 636–640, doi:10.1126/science.1087143.
- Barnes, E. A., and D. L. Hartmann, 2010: Testing a theory for the effect of latitude on the persistence of eddy-driven jets using CMIP3 simulations. *Geophys. Res. Lett.*, **37**, L15801, doi:10.1029/2010GL044144.
- , and —, 2011: Rossby-wave scales, propagation and the variability of eddy-driven jets. *J. Atmos. Sci.*, **68**, 2893–2908.
- , —, D. M. W. Frierson, and J. Kidston, 2010: Effect of latitude on the persistence of eddy-driven jets. *Geophys. Res. Lett.*, **37**, L11804, doi:10.1029/2010GL043199.
- Breiteig, T., 2008: Extra-tropical synoptic cyclones and downward propagating anomalies in the northern annular mode. *Geophys. Res. Lett.*, **35**, L07809, doi:10.1029/2007GL032972.
- Chan, C. J., and R. A. Plumb, 2009: The response to stratospheric forcing and its dependence on the state of the troposphere. *J. Atmos. Sci.*, **66**, 2107–2115.
- Chen, G., and I. M. Held, 2007: Phase speed spectra and the recent poleward shift of Southern Hemisphere surface westerlies. *Geophys. Res. Lett.*, **34**, L21805, doi:10.1029/2007GL031200.
- , and R. A. Plumb, 2009: Quantifying the eddy feedback and the persistence of the zonal index in an idealized atmospheric model. *J. Atmos. Sci.*, **66**, 3707–3720.
- , I. M. Held, and W. A. Robinson, 2007: Sensitivity of the latitude of the surface westerlies to surface friction. *J. Atmos. Sci.*, **64**, 2899–2915.
- Chen, P., and W. A. Robinson, 1992: Propagation of planetary waves between the troposphere and stratosphere. *J. Atmos. Sci.*, **49**, 2533–2545.

- Eichelberger, S. J., and D. L. Hartmann, 2007: Zonal jet structure and the leading mode of variability. *J. Climate*, **20**, 5149–5163.
- Fyfe, J. C., and O. A. Saenko, 2006: Simulated changes in the extratropical Southern Hemisphere winds and currents. *Geophys. Res. Lett.*, **33**, L06701, doi:10.1029/2005GL025332.
- Garfinkel, C. I., and D. L. Hartmann, 2011a: The influence of the quasi-biennial oscillation on the troposphere in wintertime in a hierarchy of models. Part I: Simplified dry GCMs. *J. Atmos. Sci.*, **68**, 1273–1289.
- , and —, 2011b: The influence of the quasi-biennial oscillation on the troposphere in wintertime in a hierarchy of models. Part II: Perpetual winter WACCM runs. *J. Atmos. Sci.*, **68**, 2026–2041.
- Gerber, E. P., 2012: Stratospheric versus tropospheric control of the strength and structure of the Brewer–Dobson circulation. *J. Atmos. Sci.*, **69**, 2857–2877.
- , and G. K. Vallis, 2007: Eddy zonal flow interactions and the persistence of the zonal index. *J. Atmos. Sci.*, **64**, 3296–3311.
- , and L. M. Polvani, 2009: Stratosphere–troposphere coupling in a relatively simple AGCM: The importance of stratospheric variability. *J. Climate*, **22**, 1920–1933.
- , S. Voronin, and L. M. Polvani, 2008: Testing the annular mode autocorrelation time scale in simple atmospheric general circulation models. *Mon. Wea. Rev.*, **136**, 1523–1536.
- Hartmann, D. L., J. M. Wallace, V. Limpasuvan, D. W. J. Thompson, and J. R. Holton, 2000: Can ozone depletion and global warming interact to produce rapid climate change? *Proc. Natl. Acad. Sci. USA*, **97**, 1412–1417.
- Held, I. M., 1975: Momentum transport by quasi-geostrophic eddies. *J. Atmos. Sci.*, **32**, 1494–1496.
- , and M. J. Suarez, 1994: A proposal for the intercomparison of the dynamical cores of atmospheric general circulation models. *Bull. Amer. Meteor. Soc.*, **75**, 1825–1830.
- Kang, S. M., L. M. Polvani, J. C. Fyfe, and M. Sigmond, 2011: Impact of polar ozone depletion on subtropical precipitation. *Science*, **332**, 951–954, doi:10.1126/science.1202131.
- Kidston, J., and E. P. Gerber, 2010: Intermodel variability of the poleward shift of the austral jet stream in the CMIP3 integrations linked to biases in 20th century climatology. *Geophys. Res. Lett.*, **37**, L09708, doi:10.1029/2010GL042873.
- , S. M. Dean, J. A. Renwick, and G. K. Vallis, 2010: A robust increase in the eddy length scale in the simulation of future climates. *Geophys. Res. Lett.*, **37**, L03806, doi:10.1029/2009GL041615.
- Kushner, P. J., and L. M. Polvani, 2004: Stratosphere–troposphere coupling in a relatively simple AGCM: The role of eddies. *J. Climate*, **17**, 629–639.
- Leith, C. E., 1975: Climate response and fluctuation dissipation. *J. Atmos. Sci.*, **32**, 2022–2026.
- Limpasuvan, V., and D. L. Hartmann, 2000: Wave-maintained annular modes of climate variability. *J. Climate*, **13**, 4414–4429.
- , D. W. J. Thompson, and D. L. Hartmann, 2004: The life cycle of the Northern Hemisphere sudden stratospheric warmings. *J. Climate*, **17**, 2584–2596.
- Lorenz, D. J., and D. L. Hartmann, 2001: Eddy–zonal flow feedback in the Southern Hemisphere. *J. Atmos. Sci.*, **58**, 3312–3326.
- Newman, M., and P. D. Sardeshmukh, 2008: Tropical and stratospheric influences on extratropical short-term climate variability. *J. Climate*, **21**, 4326–4347.
- Perlitz, J., and N. Harnik, 2003: Observational evidence of a stratospheric influence on the troposphere by planetary wave reflection. *J. Climate*, **16**, 3011–3026.
- Polvani, L. M., and P. J. Kushner, 2002: Tropospheric response to stratospheric perturbations in a relatively simple general circulation model. *Geophys. Res. Lett.*, **29**, 1114, doi:10.1029/2001GL014284.
- , D. W. Waugh, G. J. P. Correa, and S.-W. Son, 2011: Stratospheric ozone depletion: The main driver of twentieth-century atmospheric circulation changes in the Southern Hemisphere. *J. Climate*, **24**, 795–812.
- Ring, M. J., and R. A. Plumb, 2007: Forced annular mode patterns in a simple atmospheric general circulation model. *J. Atmos. Sci.*, **64**, 3611–3626.
- Rivière, G., 2011: A dynamical interpretation of the poleward shift of the jet streams in global warming scenarios. *J. Atmos. Sci.*, **68**, 1253–1272.
- Robinson, W. A., 2006: On the self-maintenance of midlatitude jets. *J. Atmos. Sci.*, **63**, 2109–2122.
- Roff, G., D. W. J. Thompson, and H. Hendon, 2011: Does increasing model stratospheric resolution improve extended-range forecast skill? *Geophys. Res. Lett.*, **38**, L05809, doi:10.1029/2010GL046515.
- Shaw, T. A., J. Perlitz, and N. Harnik, 2010: Downward wave coupling between the stratosphere and troposphere: The importance of meridional wave guiding and comparison with zonal-mean coupling. *J. Climate*, **23**, 6365–6381.
- Simpson, I. R., M. Blackburn, J. D. Haigh, and S. Sparrow, 2010: The impact of the state of the troposphere on the response to stratospheric heating in a simplified GCM. *J. Climate*, **23**, 6166–6185.
- , —, and —, 2012: A mechanism for the effect of tropospheric jet structure on the annular mode–like response to stratospheric forcing. *J. Atmos. Sci.*, **69**, 2152–2170.
- Son, S.-W., S. Lee, S. B. Feldstein, and J. E. Ten Hoeve, 2008: Time scale and feedback of zonal-mean-flow variability. *J. Atmos. Sci.*, **65**, 935–952.
- , and Coauthors, 2010: Impact of stratospheric ozone on Southern Hemisphere circulation change: A multimodel assessment. *J. Geophys. Res.*, **115**, D00M07, doi:10.1029/2010JD014271.
- Song, Y., and W. A. Robinson, 2004: Dynamical mechanisms for stratospheric influences on the troposphere. *J. Atmos. Sci.*, **61**, 1711–1725.
- Sun, L., W. A. Robinson, and G. Chen, 2011: The role of planetary waves in the downward influence of stratospheric final warming events. *J. Atmos. Sci.*, **68**, 2826–2843.
- Thompson, D. W. J., and T. Birner, 2012: On the linkages between the tropospheric isentropic slope and eddy fluxes of heat during Northern Hemisphere Winter. *J. Atmos. Sci.*, **69**, 1811–1823.
- , S. Solomon, P. J. Kushner, M. H. England, K. M. Grise, and D. J. Karoly, 2011: Signatures of the Antarctic ozone hole in Southern Hemisphere surface climate change. *Nat. Geosci.*, **4**, 741–749, doi:10.1038/ngeo1296.
- Vallis, G. K., 2006: *Atmospheric and Oceanic Fluid Dynamics: Fundamentals and Large-Scale Circulation*. Cambridge University Press, 772 pp.
- Wang, S., E. P. Gerber, and L. M. Polvani, 2012: Abrupt circulation responses to tropical upper-tropospheric warming in a relatively simple stratosphere-resolving AGCM. *J. Climate*, **25**, 4097–4115.
- Yu, J., and D. L. Hartmann, 1993: Zonal flow vacillation and eddy forcing in a simple GCM of the atmosphere. *J. Atmos. Sci.*, **50**, 3244–3259.